ASEAN Journal for Science and Engineering in Materials

Journal homepage: https://ejournal.bumipublikasinusantara.id/index.php/ajsem

Experimental Analysis of rGO-V_2O_5 Nanocomposites for Sus-tainable Water Remediation Completed with Bibliometric Analysis Toward Achieving Sustainable Development Goals (SDGs)

Thamer Adnan Abdullah[1], Haneen Lateef Khaleel[1], Ammar W. Saeed[2], M. N. Mohammed[3], Qusay Al-Obaidi[1], Mukhtar Ali Hussein[1], Wassef Abbood Mhmood[1], Rashed T. Rasheed[1], Oday I. Abdullah[4,5,6]*

[1] University of Technology, Baghdad, Iraq
[2] Alkarkh University of Science, Iraq
[3] Gulf University, Sanad, Bahrain
[4] Al-Naji University, Baghdad, Iraq
[5] College of Engineering, University of Baghdad, Iraq
[6] Al-Farabi Kazakh National University, Almaty, Kazakhstan
*Correspondence: E-mail: thamer.a.abdullah@uotechnology.edu.iq

ABSTRACT

This study integrates bibliometric and experimental approaches to strengthen nanotechnology-based water remediation aligned with the Sustainable Development Goals (SDG 6: Clean Water and Sanitation). A nanosorbent composed of re-duced graphene oxide (rGO) doped with vanadium pentoxide (V_2O_5) was synthesized using a thermal doping method and characterized through XRD, FESEM, and FTIR analyses. The composite achieved 68.98% removal efficiency for me-thyl orange within 30 minutes. Kinetic and isotherm analyses confirmed pseudo-second-order kinetics and Langmuir monolayer adsorption, indicating strong chemisorption and surface homogeneity. The excellent adsorption perfor-mance is attributed to the synergistic interaction between V_2O_5 and rGO, which enhances surface area, electron transfer, and active binding sites for dye molecules. These findings demonstrate the potential of rGO–V_2O_5 nanocomposites as sustainable, low-cost materials that support smart urban water systems and contribute directly to the realization of SDG 6.

ARTICLE INFO

Article History:
Submitted/Received 03 Aug 2025
First Revised 28 Sep 2025
Accepted 13 Nov 2025
First Available online 14 Nov 2025
Publication Date 01 Sep 2026

Keyword:
Adsorption kinetics,
Adsorption,
Graphene-based adsorbents,
Langmuir isotherm,
Methyl orange,
V_2O_5/rGO nanocomposite,
Water remediation.

1. INTRODUCTION

In recent years, the development of nanostructured materials has become a leading focus in materials science and environmental engineering. Nanostructures can be fabricated in various forms (such as nanorods, nanospheres, nanosheets, nanowires, and nanocomposites), each offering distinct physicochemical properties that influence adsorp-tion, catalysis, and electronic behavior. These morphological variations enable control over surface area, porosity, and charge distribution, which are essential for enhancing the interaction between adsorbent and pollutant molecules. Con-sequently, the exploration of such structures has accelerated as researchers aim to design multifunctional, efficient, and sustainable nanomaterials for environmental remediation (Kolya & Kang, 2024; Homaeigohar, 2020).

This progress is strongly aligned with the Sustainable Development Goals (SDGs), particularly SDG 6: Clean Water and Sanitation, which emphasizes universal access to safe and clean water through innovative technologies. Despite the rise of digital water monitoring systems that employ sensors and automation, their success relies fundamentally on high-performance nanomaterials capable of adsorbing and degrading contaminants (Kolya & Kang, 2024).

Industrialization continues to aggravate water contamination through the uncontrolled discharge of synthetic dyes, which are chemically stable, highly visible, and toxic to aquatic ecosystems (Deletic & Wang, 2019; Homaeigohar, 2020). These dyes, especially methyl orange (MO), persist in wastewater due to their resistance to natural degradation and their widespread use in textile, paper, and plastic industries. Exposure above 50 mg/kg can cause severe health disorders (Homaeigohar, 2020; Juzsakova *et al*., 2023).

Conventional treatment methods (including biological degradation (Gong *et al*., 2013), biosorption (Ramutshat-sha-Makhwedzha *et al*., 2022), membrane separation, and sonication (Nguyen *et al*., 2018) often fail to achieve complete removal due to operational limitations (Lv *et al*., 2019). Adsorption, in contrast, offers simplicity, cost-effectiveness, and adaptability, making it a preferred method for industrial wastewater purification (Ramutshatsha-Makhwedzha *et al*., 2022; Lv *et al*., 2019).

Among the nanostructured adsorbents, metal oxides such as vanadium pentoxide (V_2O_5), aluminum oxide (Al_2O_3), titanium dioxide (TiO_2), and iron oxide (Fe_2O_3) have demonstrated strong adsorption and catalytic activity (Ezzatfar *et al*., 2022; Hien *et al*., 2021; Xie *et al*., 2021; Jaseela *et al*., 2019; Chaukura *et al*., 2017). V_2O_5 in particular exhibits broad oxidation capability, high catalytic efficiency, and stability across a wide pH range (Abdul-Zahra & Rasheed, 2023). Meanwhile, graphene-based nanostructures, especially reduced graphene oxide (rGO), provide exceptional surface area (≈2600 m^2/g), electrical conductivity, and tunable functional groups conducive to π–π and hydrogen bonding interac-tions (Shi *et al*., 2022; Sharma *et al*., 2013).

This study focuses on the synthesis and characterization of a vanadium pentoxide-modified reduced graphene ox-ide (rGO–V_2O_5) nanocomposite prepared by a thermal doping process. The composite merges the oxidative power of V_2O_5 with the high surface area and conductivity of rGO, producing a synergistic structure that enhances adsorption capacity, electron transfer, and chemical stability. These characteristics are expected to achieve faster and more efficient dye removal through chemisorption mechanisms.

The novelty of this work lies in the integration of vanadium-based metal oxide with graphene nanosheets to form a multifunctional hybrid structure optimized for sustainable and smart urban water remediation. Furthermore, the re-search is supported by bibliometric

analysis, which identifies growing global attention toward graphene–metal oxide nanostructures for wastewater treatment, validating the relevance and timeliness of this study within current scientific trends.

2. METHODS

2.1. Materials

Ammonium-metavanadate (NH_4VO_5, 99.99%)., cetyltrimethylammonium bromide (CTAB, $C_{19}H_{42}BrN$, 99%)., and ethanol (99.8% purity) were obtained from Merck Kft., Budapest, Hungary., Sodium hydroxide (NaOH) from Merck Kft., Hydrochloric acid (HCl), from Merck Kft., Reduced graphene oxides nanosheet was purchased from USA, and used for the experiments in the present research.

2.2. Preparation of vanadium pentoxide nanoparticles

Vanadium pentoxide nanoparticles were prepared using the hydrothermal method. In this process, 0.1 g ammonium metavanadate and 0.1 g cetyltrimethylammonium bromide (CTAB) were dissolved in the mixed solvent of 7:3 ratios of ethanol and water to 100 mL. The resulting acid extract was carefully neutralized with nitric acid, and the pH was adjusted to 2.5. The reaction mixture was refluxed at 80 °C for 6 h. The formed precipitate was orange and washed ten times with distilled water and then with ethyl alcohol. The product was dried in an oven at 90 °C for nearly 1 h and calcined at 500 °C for 2 h The formation of vanadium pentoxide is shown in Equation (1) (Sharma *et al*., 2013):

$$2NH_4VO_3 + 2HNO_3 + nH_2O \xrightarrow{Ethanol/CTAB} V_2O_5nH_2O + 2NH_4NO_3 + H_2O \quad (1)$$

2.3. Synthesis of vanadium pentoxide modified (Juzsakova *et al*., 2023) nanosheet

The nanocomposite was prepared by doping vanadium pentoxide (V_2O_5) onto reduced graphene oxide (Juzsakova *et al*., 2023). 5 wt% V_2O was introduced into the reduced graphene surface, and the resulting mixture was blended using sonication for 15 min. The mixture was carefully moved to a stainless-steel Teflon autoclave reactor and cured at 200 °C in a muffle furnace.

2.4. Characterization of prepared samples

Characterization of prepared samples techniques X-ray diffraction (XRD) Patterns were recorded on a Shimadzu X-ray 6100 produced in Japan with a Cu-Kα (λ = 0.14506 nm) radiation source at 35 kV and 10 mA. The surface morphology of the nanoparticle was investigated by a Field Emission Scanning Electron Microscope (FESEM) Instrument, FEI Company product made in Poland.

2.5. Dye adsorption experiments

The absorbance at its maximum of methyl orange dissolved in water at a concentration of 20 mg/L was measured using a UV-Visible spectrophotometer (FEI Company, Poland) within the wavelength range of 400 to 700 nm. The peak absorbance (λ max) was found at 464 nm. The stock solution was subsequently employed to prepare calibration standards for UV-Vis analysis at various concentrations of methyl orange (Obayomi *et al*., 2023; Shankar *et al*., 2024). The depollution experiments for methyl orange were conducted in batch mode as previously described (Obayomi *et al*., 2023; Shankar *et al*., 2024). The stock solutions of methyl orange were diluted with distilled water, and the pH value of the dye solution was

adjusted to pH = 7 by 0.1 N NaOH or 0.1 N HCl. In each experiment, 20 mg of metal oxides modified rGO was mixed with 30 mL of dye solution (20 mg/L). The adsorption of methyl orange was studied by investigating the contact time. The adsorption process was stopped, and samples were taken for separation using a centrifuge. A UV-Visible spectrometer was employed to measure the dye concentration in the supernatant. The absorbance determined the equilibrium adsorption capacity of removal at 464 nm. Removal efficiency (RE%) of methyl orange was computed by comparing the initial and final concentrations as shown in Equetion (2) (Obayomi *et al*., 2023; Shankar *et al*., 2024):

$$RE = \left(\frac{C_0 - C_t}{C_0}\right) \cdot 100\ \% \quad (2)$$

Where (C0) is the initial concentration (mg L−1) of methyl orange (MO), (Khan *et al*., 2022) is the concentration (mg L−1) of MO at time (t), and qt is the MO adsorbed, calculated from (3). (Obayomi *et al*., 2023; Shankar *et al*., 2024):

$$q_t = \frac{(C_\circ - C_t)}{m} \cdot V \quad (3)$$

Where V was the volume of the solution (L), m was the mass of the prepared vanadia-modified graphene (g), and qt denoted the adsorption amount of MO at time t (mg/g). Triplicates were carried out under the same conditions, and averages were determined and illustrated in the paper. **Figure 1** explains the processes of the lead ions removal from aqueous solution.

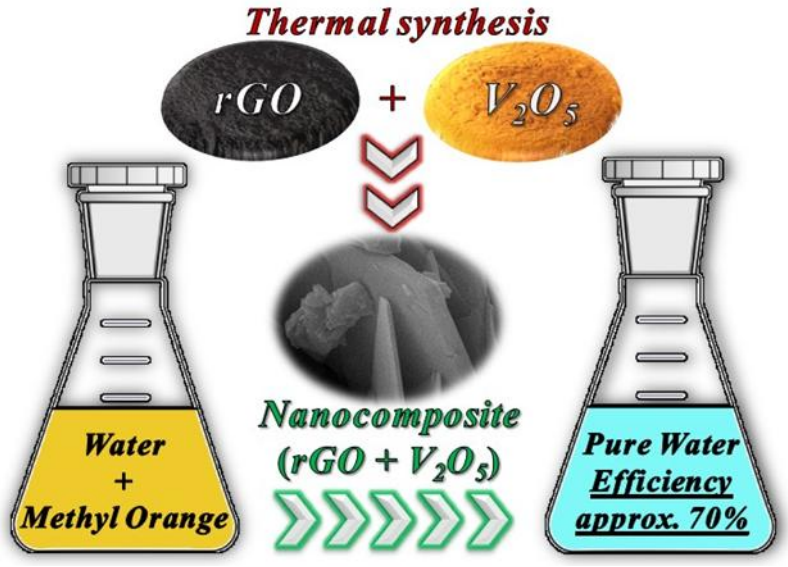

Figure 1. The nano sorbent process for lead ion removal from aqueous solution.

3. RESULTS AND DISCUSSION

3.1. XRD Results

The X-ray diffraction (XRD) technique identifies and understands the crystalline structure and growth characteristics of reduced graphene oxides (Juzsakova *et al*., 2023). The XRD pattern of the samples, depicted in **Figure 2**, shows a typical diffraction peak that corresponds to the (002) plane, which is highly indicative of reduced graphene oxide (Juzsakova *et al*., 2023; Rasheed *et al*., 2021). This peak usually appears around 26° (2θ), suggesting partial restoration of the graphitic structure after the reduction process. This peak corresponds to the highly ordered layered structure exhibiting an interlayer spacing of 0.33 nm along the

(002) orientation, confirming the presence of a well-organized hexagonal lattice. The presence of the (002) peak in the reduced graphene oxide samples suggests that the reduction process has successfully reintroduced some degree of graphitic ordering. However, residual defects and oxygen groups may still exist. This partial restoration is characteristic of rGO, where the hexagonal structure is reformed but not to the same extent as in pristine graphite. Figure 1 illustrates the primary diffraction peaks of V_2O_5 as prepared at 90 °C, with 2θ values of 15.62°, 31.4°, 40.9°, 50.5°, and 58.8°. These peaks match the characteristic diffraction patterns of the (200), (110), (310), (002), and (611) planes of V_2O_5, respectively (Aldabagh *et al*., 2024).

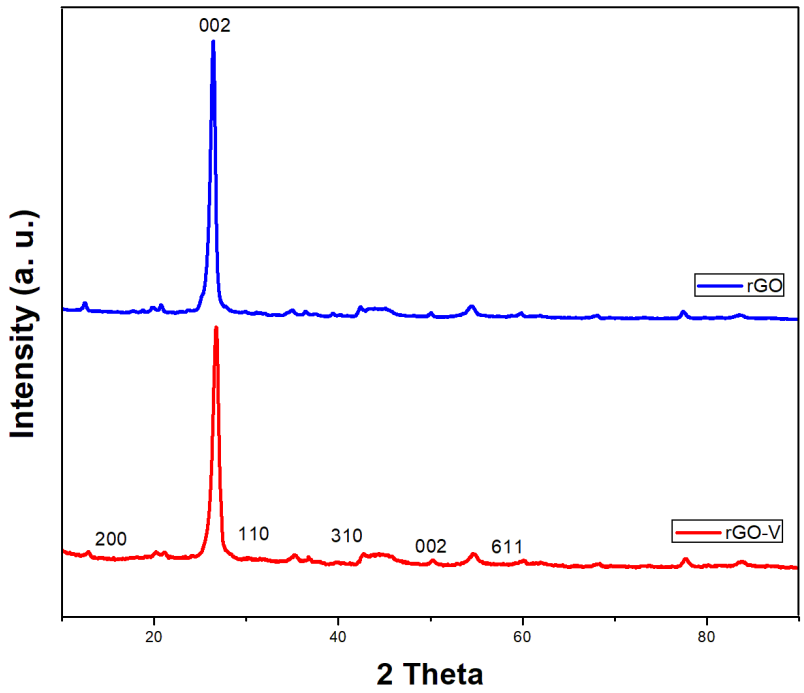

Figure 2. The XRD analysis of rGO and V_2O_5 modified rGO.

3.2. FESEM and EDX results

Figure 3 illustrates the morphology of a few-layer reduced graphene oxide (Juzsakova *et al*., 2023) nanosheet before oxidation, representing a thin, homogeneous layer of reduced graphene oxide film. Figure 3a is the low magnification of the SEM image, whereas Figures 3b and c are the high magnification of the SEM images. The images also show that the few-layer reduced graphene oxide material contains multiple layers arranged on each other in a paper-like structure, with wavy folded sheets. Moreover, this material has a sharp edge, indicating the successful reduction process while maintaining a layered morphology. These figures show images of reduced graphene oxide nanosheets with more stacked layers, with larger folds and wrinkles. This indicates that the reduction process significantly influences the structural arrangement, increasing interlayer spacing and forming thicker multilayered structures.

Figure 4 shows FESEM images of vanadia nanosize and a nanocomposite of reduced graphene oxide and vanadium pentoxide (V_2O_5) nanosheets. **Figure 4a** shows an FE-SEM image of vanadium pentoxides, which were prepared in small sheets with a nanoscale between 49 and 68 nm. **Figures 4b and c** illustrate the size and shape of the V_2O_5 nanoparticles intercalated with the reduced graphene oxide nanosheets. The average

diameter of the V_2O_5 nanoparticles was determined to be 59 nm. Successful incorporation of V_2O_5 nanoparticles within the reduced graphene oxide matrix enhances the composite's structural stability and surface area, potentially improving its electrochemical performance.

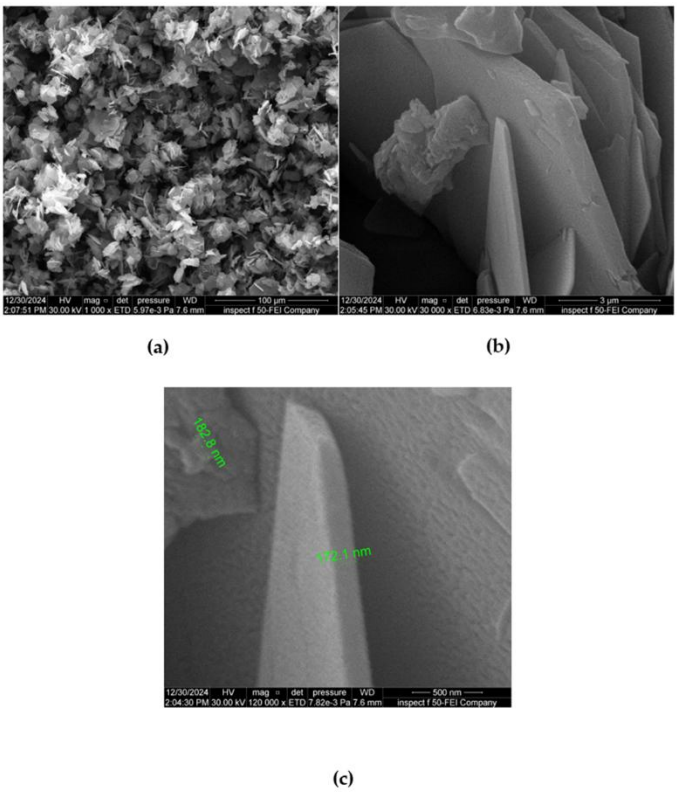

Figure 3. FESEM images of rGO nanosheet at several magnifications of (a) 100 µm, (b) 3 µm, and (c) 500 nm.

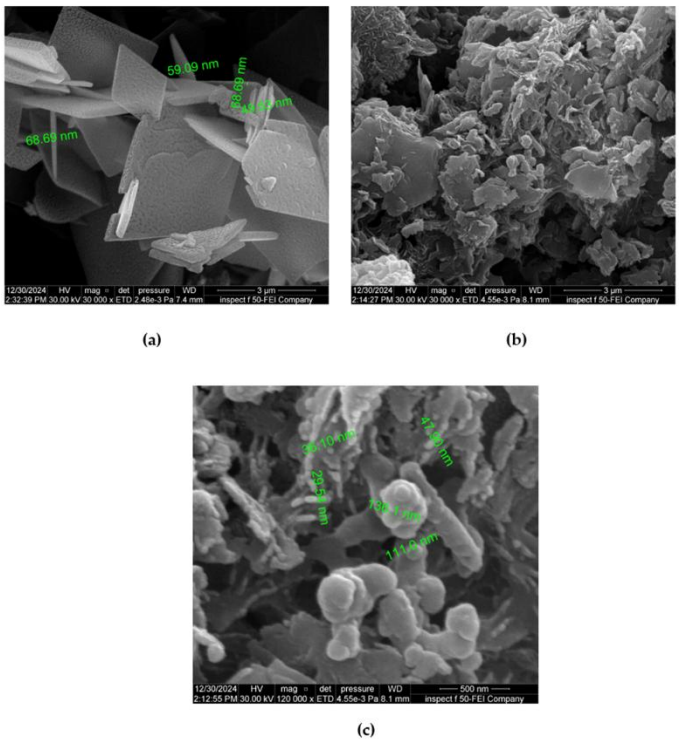

Figure 4. FESEM image of vanadium pentoxide nanosize (a) FE-SEM images of V_2O_5-rGO nanocomposite at several magnifications of 3 µm (b), and 500 nm (c).

EDX analysis confirmed the elemental composition of reduced graphene oxide (rGO, **Table 1**) and the vanadia-functionalized composite (rGO-V, **Table 2**). Following functionalization, the carbon content decreased from 90.9 wt% to 78.3 wt%, while the oxygen content increased from 9.1 wt% to 14.4 wt%. Furthermore, vanadium was detected in the composite at 4.3 wt%. These compositional changes indicate the successful integration of vanadia species onto the rGO surface.

Table 1. EDX results of rGO.

Element	Atomic %	Atomic % Error	Weight %	Weight % Error
C	93.0	0.8	90.9	0.8
O	7.0	0.7	9.1	0.9

Table 2. EDX results of rGO-doped vanadium pentoxide.

Element	Atomic %	Atomic % Error	Weight %	Weight % Error
C	85.9	1.3	78.3	1.2
O	09.9	0.7	14.4	0.9
Mg	0.2	0.1	0.4	0.1
Al	0.0	0.0	0.1	0.1
Si	0.2	0.0	0.3	0.1
Cl	0.3	0.0	0.8	0.1
K	0.3	0.1	1.0	0.2
V	3.6	0.0	4.3	0.1
Ni	0.5	0.1	2.3	0.4

3.3. FTIR Spectra for rGO, rGO-V, and rGO-V after Methyl Orange Adsorption

The FTIR spectra of fresh reduced graphene oxide (Juzsakova *et al*., 2023), vanadia-loaded reduced graphene oxide (rGO–V), and the nanosorbent after methyl orange (MO) adsorption (rGO–V+MO) (**Figure 5**) provide compelling evidence for the successful synthesis of the hybrid nanomaterial and subsequent dye adsorption, while also elucidating the underlying chemical interactions. The transformation from the pristine rGO spectrum to that of rGO–V confirms two fundamental processes:

(i) Reduction of the graph- oxide: The impacts of oxygen-containing feature band strength are found in **Figure 5**. Some characteristic bands, such as that at 1720 cm^{-1}, being due to C=O stretching and the C–OH bending band of 1220 cm^{-1}, or finally the C–O stretch vibration from 1050 cm^{-1}, all either dropped radically in intensity or disappeared altogether (**Figure 5**). This clearly shows that GO has undergone efficient chemical reduction to rGO through treatment with V_2O_5; these changes are done traceably in parallel with the load-carrying out procedure.

(ii) Species introduction: New characteristic vibration peaks arose after vanadia loading, indicating that products such as V_2O_5 were formed. A sharp, intense band beginning at 1020 cm^{-1} corresponds to the out-of-plane stretching mode of terminal V=O; additional bands within a range of 600-800 cm^{-1} can all be attributed to V–O–V bridging vibrations between different oxide units in vanadialatis. Also, the O–H stretching band (3200- finally split into two parts: a broadly shaped part beginning from around 3200 cm^{-1} and extending up to 3400 cm^{-1}; a sharp band between these two ranges of values soon developed Its (**Figure 5**), clearly pointing out changes in shape and intensity that are characteristic of a V_2O_5 nanoparticle's interaction with edges of residual hydroxyl

groupson rGO surface. Collectively, these spectral modifications confirm both the reduction of GO and the successful immobilization of V_2O_5 on the carbonaceous matrix.

(iii) The spectral changes after exposure to methyl orange (MO) confirm successful adsorption and provide clues about the adsorption mechanism: The broadening of the O-H stretching peak suggests that hydrogen bonding between the dye and hydroxyl groups on the composite surface is also a contributing factor to the adsorption process. The spectrum of the rGO-V+MO composite shows new peaks characteristic of methyl orange. A peak in the range of 1550-1600 cm^{-1} can be assigned to the azo group (-N=N-) stretching vibration (though it may overlap with the C=C stretch from the carbon backbone). Peaks in the regions 1000-1100 cm^{-1} and 1150-1250 cm^{-1} indicate the sulfonate group ($-SO_3^-$) vibrations. The most significant evidence is the shift and decrease in intensity of the vanadia peaks (V=O at 1020 cm^{-1} and V-O-V at 600-800 cm^{-1}). This indicates a strong chemical interaction, likely through coordination between the dye molecules (lone pairs of electrons on the azo group (-N=N-) and sulfonate group ($-SO_3^-$), which react as Lewis bases) and the vanadium (empty orbitals which react as Lewis acids) sites on the nanoparticle surface. The broadening of the O-H stretching peak suggests that hydrogen bonding between the dye and hydroxyl groups on the composite surface is also a contributing factor to the adsorption process (see **Figure 5**).

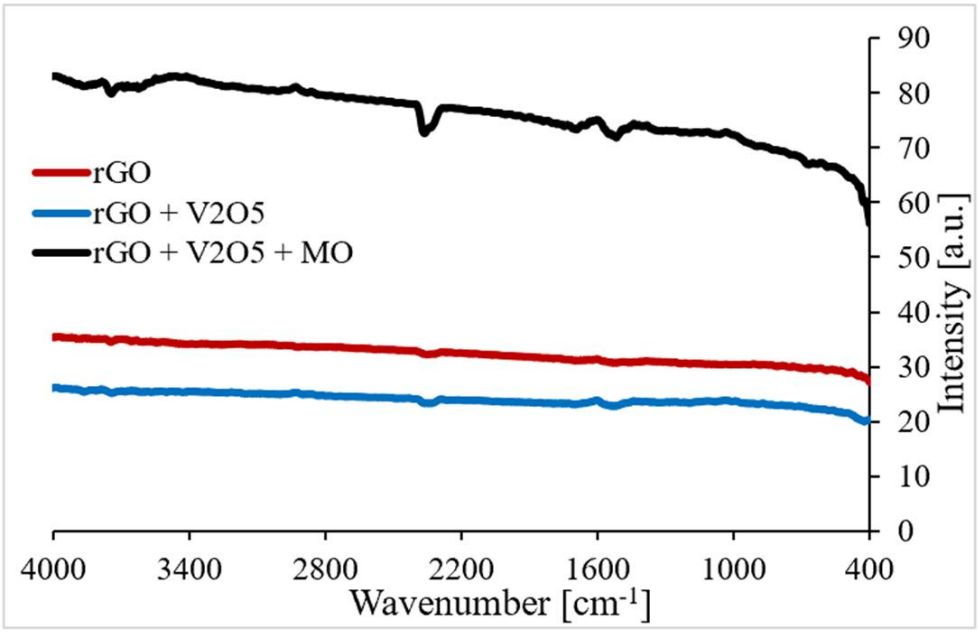

Figure 5. FTIR spectra of pristine rGO nanosheets, vanadia-modified rGO (rGO-V), and rGO-V after methyl orange (MO) adsorption.

Moreover, the broadening of the O–H stretching band (3200–3400 cm^{-1}) after adsorption supports the involvement of hydrogen bonding between the hydroxyl groups of the composite and functional moieties of the dye. This dual interaction—Lewis acid–base coordination and hydrogen bonding—facilitates adsorption and alters the local electron density around vanadium, thereby weakening the V=O bond. The resulting downshift and diminished intensity of the V=O stretching band completely agree with the observed spectral changes (**Figure 6**).

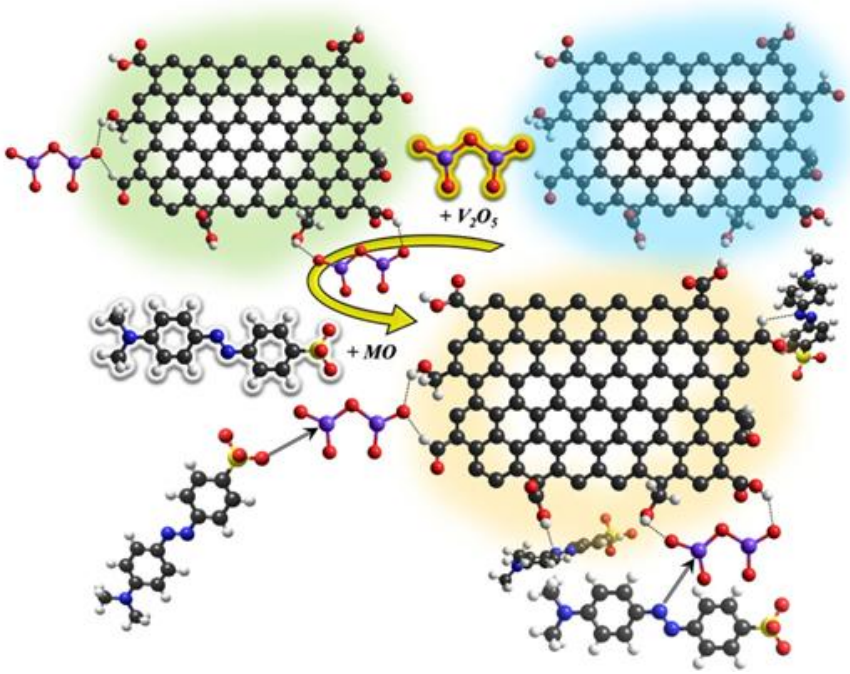

Figure 6. Proposed mechanism of MO adsorption over rGO-V.

3.4. Adsorption Results of MO removal using rGO and rGO-V

After their preparation and doping, a study was conducted on reduced graphene oxide (Juzasakova *et al.*, 2023) and reduced graphene oxide modified with vanadium pentoxide nanoparticles (rGO-V). The study aimed to remove MO dye from water, an organic dye that pollutes water and negatively impacts the aquatic environment. The removal of methyl orange (MO) dye from water was studied. MO is also an organic dye that contributes to water pollution and negatively impacts the aquatic environment. Given its harmful environmental impacts, this study aimed to evaluate the efficiency of nano-adsorbents in removing this dye. A starting concentration of methyl orange was 20 mg/L, and the solution volume for each adsorption experiment was 30 ml. Adsorption time ranged from 0 to 50 minutes, with absorbance measured using UV-Vis spectroscopy every 10 minutes. The nano-adsorbent was 10 mg, and all experiments were conducted at 25 °C. These experimental conditions were carefully selected to ensure the adsorbent's performance in dye removal could be evaluated under conditions resembling real-world environmental applications. The results of methyl orange removal are presented in **Figures 7 and 8** and in **Table 3**. **Figure 7** shows that the methyl orange concentration gradually decreased with adsorbent time, reaching 9.48 and 6.40 mg/L for rGO and rGO-V, respectively, after 30 minutes. **Figure 8** shows the adsorption efficiency, with the highest efficiency recorded after 30 minutes, reaching 53.09% and 6.22 % for rGO and rGO-V, respectively. These results are clearly shown in **Figure 8** and **Table 3**. This study confirms the efficiency of the nano-adsorbent in removing methyl orange dye, highlighting its potential for application in the treatment of dye-contaminated water. Note that doping V_2O_5 nanosize over rGO resulted in better methyl orange removal results from water compared to reduced graphene oxide.

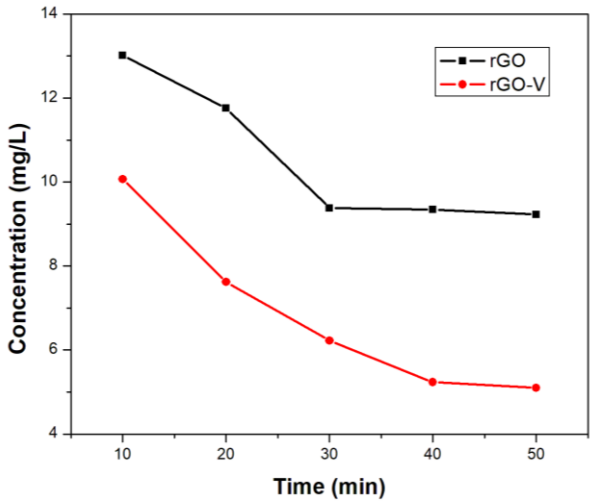

Figure 7. Change in MO concentration against time over rGO and rGO-V nanosheets.

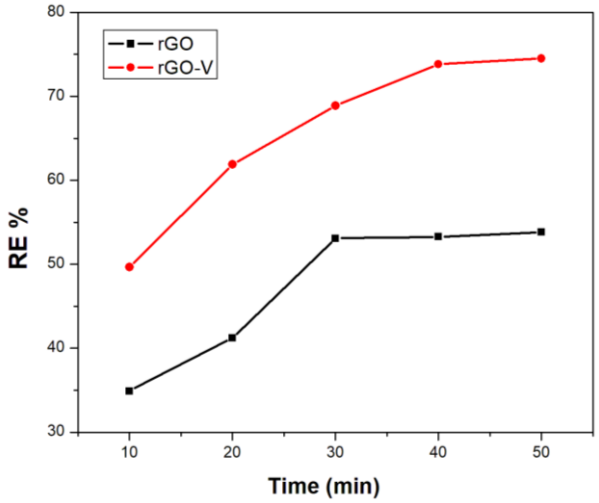

Figure 8. Time-Dependent Removal Efficiency (RE%) of MO from Water Using rGO and rGO-V nanosheets.

Table 3. MO removal efficiency and reduction in concentration using rGO and rGO-V.

	r-GO-V				**r-GO**		
T (min)	**C (mg/L)**	**RE %**	**qe mg/g**	**T (min)**	**C (mg/L)**	**RE %**	**qe mg/g**
10	10.11	49.40	29.64	10	13.61	31.91	19.15
20	7.65	61.71	37.02	20	11.31	43.41	26.046
30	6.40	67.95	40.77	30	9.48	52.59	31.55
40	6.13	69.33	41.59	40	9.256	53.71	32.22
50	5.12	74.39	44.63	50	9.15	54.21	32.52

Finally, the effect of pH on the removal efficiency of lead ions from aqueous solutions using the synthesized nano-adsorbent vanadia-doped graphene oxide was systematically investigated across a pH range of 3, 5, 7, 9, and 11, as shown in **Figure 9**. After statistical processing, how acidic conditions by the lead ion adsorption effect are best, appeared at pH 5 maximum removal efficiency is 82%, trumping that achieved at pH 3 with 78%. But under neutral and alkaline conditions (pH 7, 9, and 11), adsorption efficiencies were all relatively low. Specifically, the least removal was observed under pH 9 and 11, so it goes without saying

that if one wishes to remove lead ions, then they should tune a synthesized nano-adsorbent toward moderate acidity. All these effects are the central issues around which this research has been built. This is because one of the most valuable features in lead remediation from polluted waters with powdered ash as sorbent material (hereafter, 'nano-adsorbent') comes from its increased surface charge interactions, facilitating absorption and adsorption of ions. Based on these findings, it is evident that the application of the nano-adsorbent must be put at each pH rather than using creation (for instance, at lower pH) to reach better lead removal from water polluted with real estate waste site effluents.

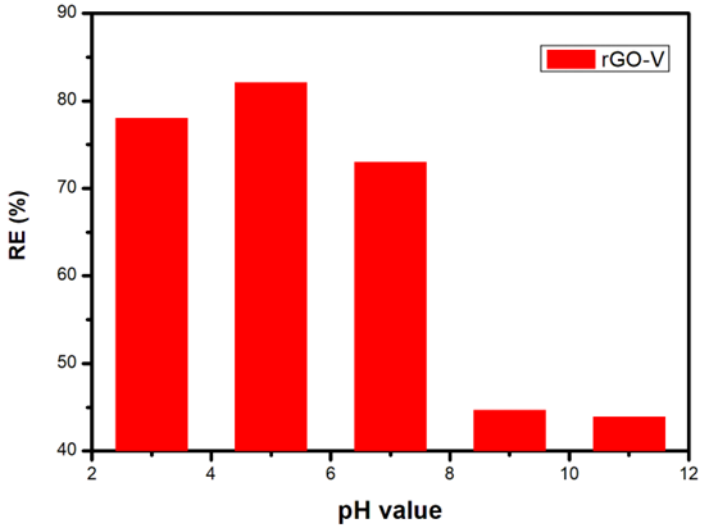

Figure 9. Influence of Solution pH on the Lead Ion Removal Efficiency Using rGO-V Nano-Adsorbent.

3.5. Reusability of the Nano-Adsorbent for Lead Ion Removal

The aim of this step of research was to systematically test the reusability of the nanosorbent through a multi-step regeneration process, to maintain continuous and effective adsorption performance. In the first step, the nanoparticles were dispersed in distilled water and subjected to high-speed shaking. The solution was centrifuged, separating the adsorbent from the solvent. Each time this cleaning activity occurred twice or more, it could remove impurities effectively. Subsequently, the nano-adsorbent was treated with a NaOH solution of 0.1 M under constant stirring to elute absorbed lead ions. The nanoparticles were recovered by centrifugation. To remove residual organic substances remaining on the surface of the adsorbent, the nanoparticles were mixed with a 20% ethanol solution, thoroughly shaken, and finally centrifuged. This last washing step was repeated with distilled water to remove any traces of solvents completely. Finally, the regenerated nano-adsorbent was dried in an oven at 100 °C to restore its physicochemical properties and prepare it for further adsorption cycles. Such a reactivation scheme is necessary for successful reproductions of removing lead ions from aqueous solution through this type of nano-adsorbent (see **Figure 10** gives details of the method and outcome).

The reusability of the synthesized nano-adsorbent was rigorously assessed over four consecutive adsorption-desorption cycles. The adsorption efficiency remained at approximately 74% relative to the initial removal efficiency before regeneration, indicating full performance retention during the first three cycles. A slight decrease in removal efficiency to approximately 90% of the original capacity was observed in the fourth cycle, demonstrating

a minor loss in adsorption efficiency of lead ions from aqueous solution. These results highlight the excellent structural stability and preservation of active sites of the nano-adsorbent, confirming its robustness and suitability for repeated application in the remediation of lead-contaminated aqueous solutions.

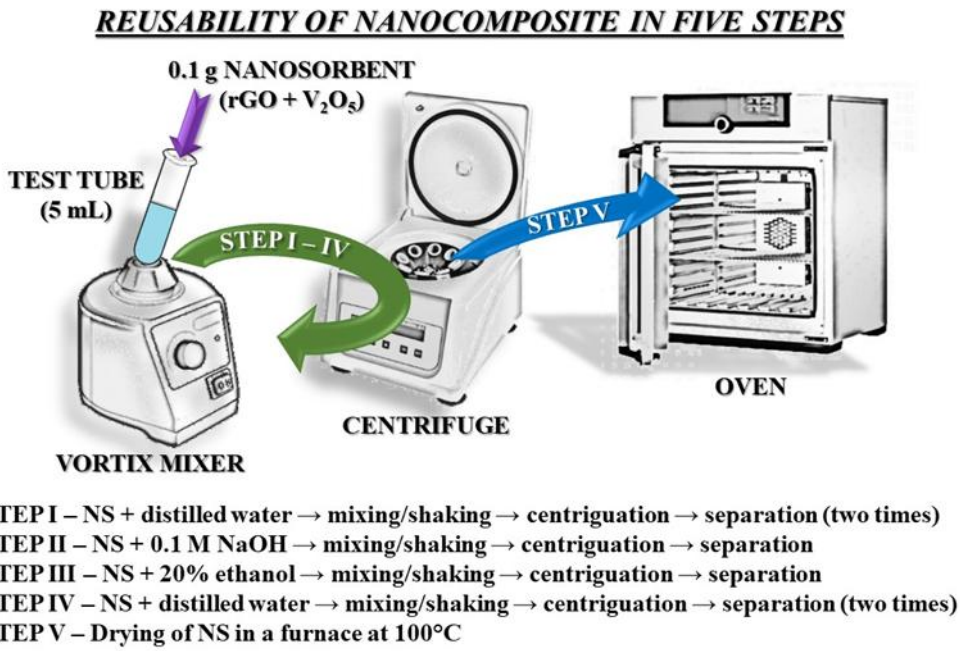

Figure 10. Regeneration procedure of the nanosorbent for repeated Lead ion removal from aqueous solutions.

3.6. Adsorption kinetics of MO removal using r-GO and r-GO-V.

The pseudo-first order reaction rate constant was determined using Equation (4) (Aldabagh *et al*., 2024):

$$\log(qe - qt) = \log qe - k_1 t / 2.303 \quad (4)$$

Where qe (mg g^{-1}) and qt(mg g^{-1}) are the adsorption capacities of MO at the equilibrium and at time t(min), respectively, and k1 is the first-order rate constant (min^{-1}). Slope and intercepts of plots of log (qe − qt) were (t) used to determine (k_1) and (Mashhour *et al*., 2024) for both r-GO and vanadia-modified r-GO (r-GO-V). As demonstrated in **Figure 11**, the pseudo-first order reaction for the r-GO and r-GO-V has the coefficient of determination (R^2) of 0.8174 and 0.8995, respectively, as in **Figures 11 (a and b)**. The pseudo-second order equation, which depends on the equilibrium capacity adsorption, can be represented by Equation (5).

$$t/qt = 1/k_2 q^2 e + t/qe \quad (5)$$

In Eq. 5, (k2) refers to the second-order adsorption rate constant (g/mg · min). The slopes and intercepts of the straight-line plots of (t/qt) versus (t) were used to obtain the values of (Mashhour *et al*., 2024) and (k_2). The sorption of methyl orange (MO) onto both reduced graphene oxide (r-GO) and vanadia-modified reduced graphene oxide (r-GO-V) was described by the pseudo-second order model. The pseudo-second order model represents a better fit of the experimental data of MO adsorption since the determination coefficients (R^2) for r-GO-V were higher than those for the pseudo-first order model for r-GO-V. However, the R2 of the pseudo-second order model for r-GO-V is higher than that for r-GO. (R_2 = 0.9643 and 0.7754) (**Figures 12 (c and d**)). The diffusion model was used to determine the mechanism of diffusion

in the system, using the parameters obtained from the third kinetic intraparticle diffusion model established by Weber–Morris. The initial intra-particle diffusion rate can be expressed as Equation (6) (Aldabagh *et al*., 2024).

$$qt = K_d\, t\, 1/2 + C \quad (6)$$

According to the intra-particle diffusion model, the diffusion constant K_d (mg/g·min$^{1/2}$) and the intercept C are critical parameters describing the adsorption mechanism. In this framework, the amount of adsorbate the sorbent (qt) takes up is expected to vary linearly with the square root of contact time ($t^{1/2}$). The results of this kinetic model are illustrated in **Figures 12 (e) and 12(f)**. The K_d values were determined from the slopes of the plots of qt versus $t^{1/2}$. The linear plots did not intersect the origin, with correlation coefficients (R^2) of 0.9518 for r-GO and 0.9357 for r-GO-V, indicating that intra-particle diffusion is not the sole rate-limiting step.

The deviation from the origin suggests the influence of boundary layer effects, as reflected by the intercept values. Specifically, the C and K_d values were 6.1295 and 18.4280 for r-GO, and 4.3449 and 3.8747 for r-GO-V, respectively. A higher C value indicates a more pronounced boundary layer resistance, highlighting the significance of surface sorption in controlling the adsorption rate. A summary of these parameters is provided in **Table 4**.

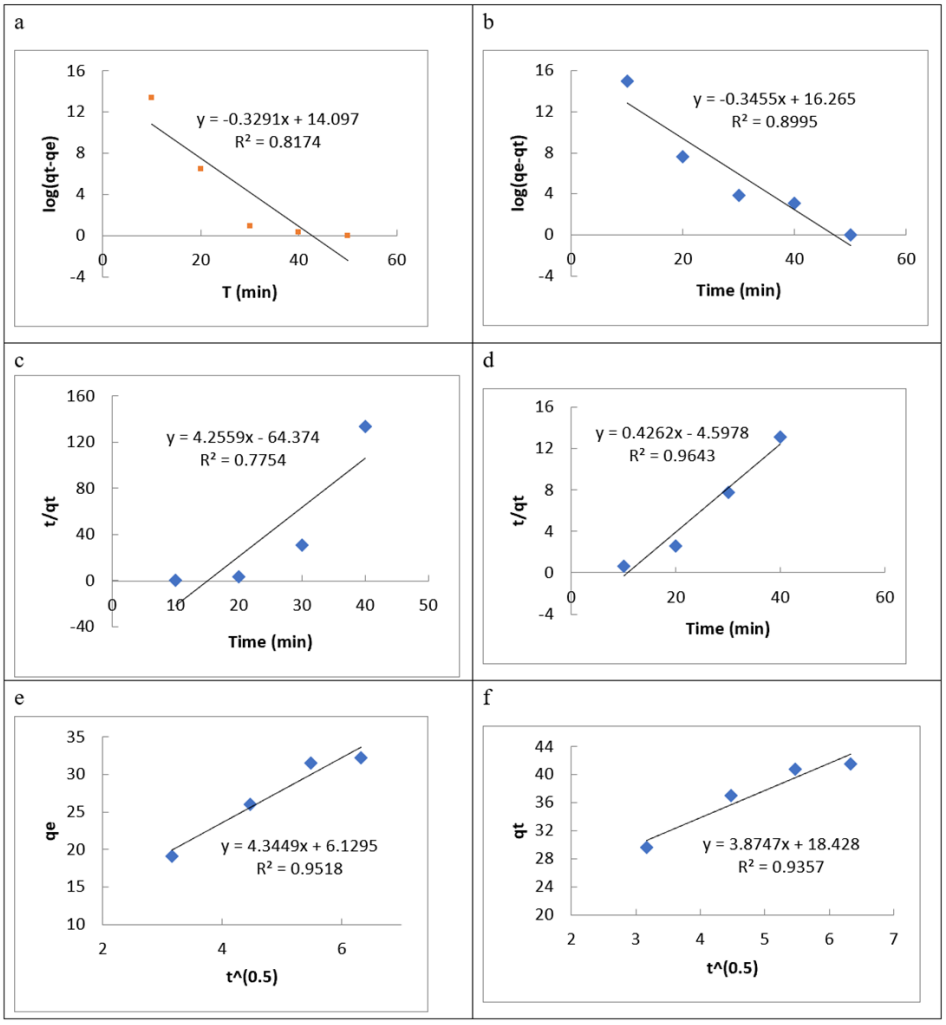

Figure 11. Pseudo-first-order plot (a, b), pseudo-second-order plot (c, d), intra-particle diffusion plot (e, d) for MO adsorption onto r-GO and a-GO-V, respectively.

Table 4. Comparison of Kinetic Model Equations for the Sorption of Methyl Orange (MO) onto r-GO and r-GO-V.

Pseudo-First Order			Pseudo-Second Order			Intra-Particle Diffusion		
K_1 (min^{-1})	qe cal (mg/g)	R^2	k_2 (g/mg min)	qe cal (mg/g)	R^2	Kd (mg/g $min^{1/2}$)	C	R^2
0.7579	1.14913	0.8174	0.0395	0.2349	0.7754	4.3449	6.1295	0.9518
0.7957	1.2113	0.8995	0.0395	2.3463	0.9643	3.8747	18.428	0.9357

3.7. Adsorption isotherm of MO removal using r-GO and r-GO-V.

The applicability of the Langmuir and the Freundlich isotherms for methyl orange (MO) was evaluated by plotting (Ce/qe) versus (Ce) (as described in Equation (7)) and (log qe) versus (log Ce) (as outlined in Equation (8)), respectively (Fathi *et al*., 2024).

$$\frac{Ce}{qe} = \frac{1}{KLqmax} + \frac{Ce}{qmax\ b} \tag{7}$$

Here (Ce) is the concentration of the pollutant in the solution at equilibrium, (mg/L); (Mashhour *et al*., 2024) is the mass of Methyl orange (MO) that is adsorbed by the sorbent at equilibrium, (mg/g). Also, q max is the maximum tested amount of pollutant that can be adsorbed per unit weight of the sorbent (mg/g), and b is the Langmuir adsorption equilibrium constant (L/mg), which is a measure of adsorbent-pollutant affinity.

$$\log \mathrm{qt} = \log \mathrm{KF} + \frac{1}{n} \log Ce \tag{8}$$

In Here, (KF) and (1/n) are the Freundlich adsorption constant, (mg/g) (mg/L) 1/n and adsorption intensity, respectively. Both r-GO and r-GO-V fitted well with the Langmuir equation in the isotherm data (**Figure 12 (a) and (b)**), and R^2 values were 0.9939 and 0.9835, respectively. This suggests that the adsorption of MO was a monolayer surface reaction, and the monolayer adsorption model (Langmuir) describes it well. The value of the Freundlich parameter (n) denotes the adsorption intensity, which is 3.1949 and 10.2775 for r-GO and r-GO-V, respectively. Relaxation time was not found to obey a simple exponential law, and it did not indicate a difference in overall adsorption reported here (Higher n > 1) than physical adsorption. The adsorption isotherm of MO on r-GO-V conforms to Langmuir and presents monolayer adsorption property (Iqbal *et al*., 2017; Mahdy & al-Naseri, 2024).

Sometimes, the Flory–Huggins isotherm model (Jehad *et al*., 2024; Chu *et al*., 2023) is used to obtain the degree of surface coverage characteristics of the adsorbate on the adsorbent. It can also represent the feasibility and spontaneity of the adsorption process. (KF) and (KL) were the equilibrium constants of the Freundlich and Langmuir isotherms, respectively. The latter constants are used for spontaneous elaboration of the process by using the Gibbs free energy connected with Equation (9).

$$\Delta G^{o} = -RT\ln(K) \tag{9}$$

The parameters R, T, and K in the thermodynamic equation represent the universal gas constant (8.314 J/mol·K), absolute temperature, and the equilibrium constant KL for Langmuir or KF for the Freundlich isotherms, respectively. Based on this relationship, the calculated Gibbs free energy changes (ΔG°) for the Langmuir isotherm were −1.1127 kJ/mol and −4.5389 kJ/mol for r-GO and r-GO-V, respectively. In contrast, the corresponding values for the Freundlich isotherm were −0.5551 kJ/mol and −1.7856 kJ/mol.

As listed in **Table 5**, these values indicate that the adsorption process is thermodynamically favorable and spontaneous, particularly under the studied conditions. Compared to the Freundlich model, the more negative ΔG° values associated with the Langmuir model suggest a stronger interaction between methyl orange (MO) molecules and the adsorbents. Furthermore, the significantly more negative ΔG° value for r-GO-V relative to r-GO in the Langmuir isotherm implies that MO adsorption onto r-GO-V is more spontaneous and energetically favorable.

To know the efficiency of the adsorbent synthesized to remove methyl orange, comparisons must be made between the findings presented here and other research conducted with different adsorbents. This study's highest adsorption capacity achieved was 44.63 mg/g applying r-GO-V, which is relatively practical. To compare this result with similar adsorbents, namely silica gel (Nuraeni *et al*., 2023) LD I, MCM-48 mesoporous silica LD 0.049 mg/g (Fathi *et al*., 2024) (equilibrium fitted to Langmuir isotherm as well). One of the most common adsorbents used is activated carbon, owing to its adsorption capacity, with the CAR900 material and CA being about 15.72 and 16.90 mg/g, respectively (Taquieteu *et al*., 2023). In addition, biochar and metal oxide nanoparticles have been investigated for methyl orange adsorption, and their capacities have also changed within 37.31 and 20.53 mg/g according to their surface character and the way of synthesis (Do *et al*., 2023; Chaukura *et al*., 2017).

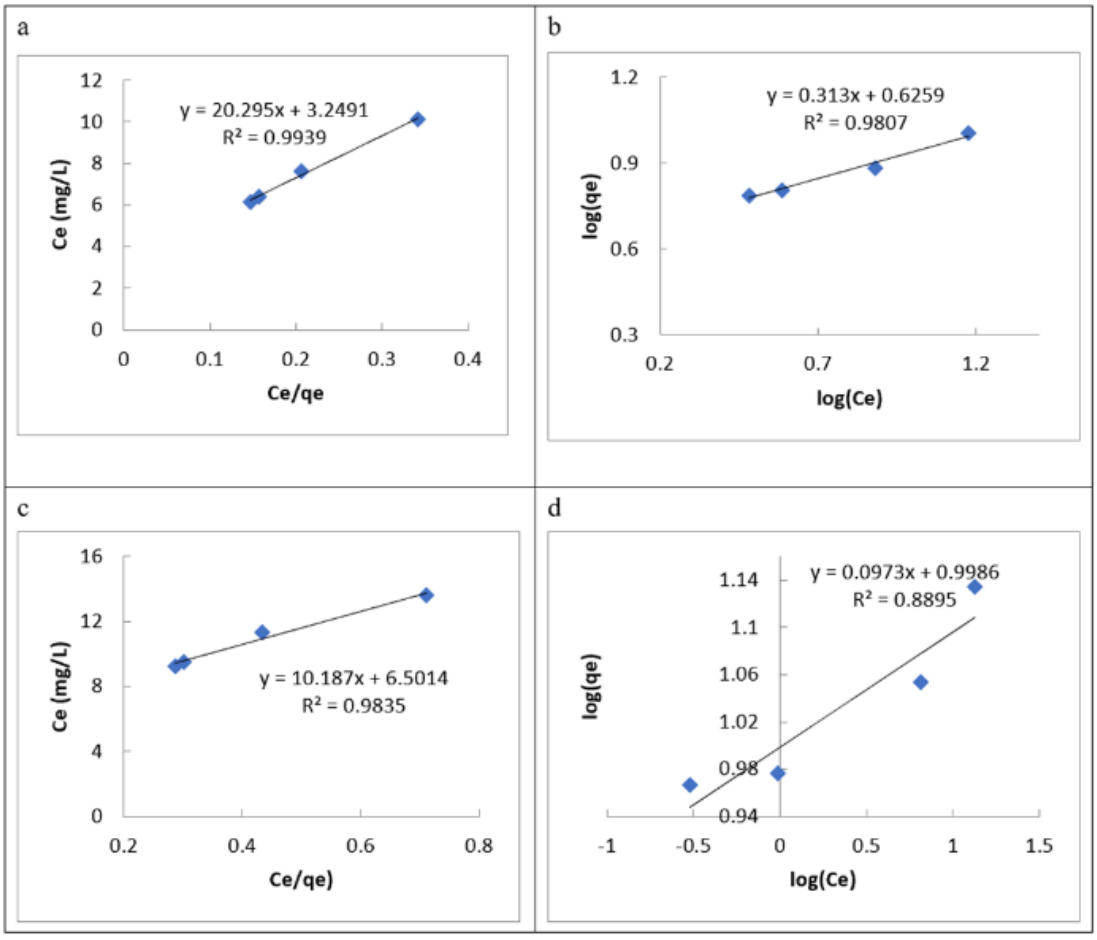

Figure 12. Isotherm models for MO adsorption on r-GO and r-GO-V (**a and b**); Langmuir and Freundlich isotherm models for MO adsorption on r-GO (c and d); Langmuir and Freundlich isotherm models for MO adsorption on r-GO-V.

Table 5. Correlation coefficients and constant parameters were calculated for various adsorption models for MO adsorption on r-GO and r-GO-V.

Langmuir				Freundlich			
qmax (min^{-1})	K_L (L/mg)	R^2	$\Delta G_L°$ (KJ/mol)	K_F (mg/g)	n	R^2	$\Delta G_F°$ (KJ/mol)
0.0982	1.5669	0.9835	-1.1127	1.2511	10.2775	0.8895	-0.5551
0.0493	6.2463	0.9939	-4.5389	2.0559	3.1949	0.9807	-1.7856

3.8. Bibliometric and SDG Relevance

A bibliometric analysis was conducted using the Scopus database with the query *TITLE-ABS-KEY ("water" AND "remediation")* covering the period 1928–2025. As shown in Figure 13, global publication activity in this domain has grown exponentially, reaching 7,599 documents in 2025, compared to only 2,027 publications in 2017, out of a total of 60,014 indexed studies. This upward trend reflects the accelerating scientific and policy focus on sustainable water management, environmental protection, and the development of advanced remediation technologies. Bibliometric has been well-used in many areas as reported elsewhere (Nandiyanto *et al*., 2025; Solehuddin *et al*., 2025; Mubarokah *et al*., 2024; Maryanti *et al*., 2022).

The bibliometric trend strongly aligns with SDGs, which call for innovative, cost-effective, and scalable solutions to ensure access to clean water and to mitigate pollution at its source. Research on nanostructured materials, particularly carbon- and metal-oxide–based composites, has dominated the field since 2020, emphasizing their role in adsorption, catalysis, and water purification applications.

Positioned within this global framework, the present study contributes to the emerging paradigm of sustainable nanotechnology-driven water remediation. By integrating bibliometric insights with experimental validation, the research confirms both its scientific novelty and global relevance, providing evidence that the development of rGO-V_2O_5 nanocomposites directly supports the progress of SDG 6 and strengthens the knowledge foundation for future smart and resilient urban water systems.

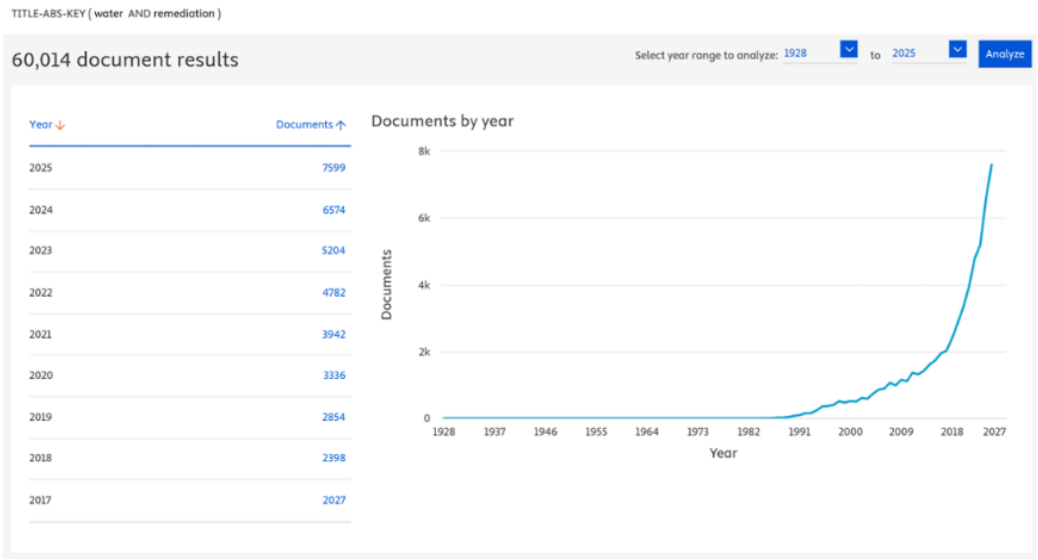

Figure 13. Annual publication trends on water remediation research based on Scopus data (1928–2025), showing exponential growth in global scientific output related to sustainable water management and nanotechnology applications. Data was taken on November 2025.

4. CONCLUSION

This study demonstrated the successful synthesis and characterization of a vanadium pentoxide–modified reduced graphene oxide (rGO–V_2O_5) nanocomposite as an effective adsorbent for methyl orange dye removal from aqueous me-dia. The composite achieved high adsorption efficiency within a short contact time, following pseudo-second-order ki-netics and Langmuir monolayer adsorption, which confirmed a chemisorption-dominated mechanism and surface ho-mogeneity. The synergistic interaction between V_2O_5 and rGO enhanced electron transfer, surface reactivity, and the density of active sites, resulting in a material that is both stable and reusable. These results signify the potential of nanostructured hybrid composites in advancing environmentally sustainable water treatment aligned with Sustainable Development Goal 6 (Clean Water and Sanitation). The work's novelty lies in integrating the oxidative capability of va-nadium pentoxide with the conductive, high-surface-area characteristics of graphene to form a multifunctional, eco-efficient nanomaterial for smart urban water systems. Additionally, bibliometric analysis supports the relevance and timeliness of this research, situating it within a growing global trend toward graphene–metal-oxide nanostructures for sustainable wastewater remediation.

5. AUTHORS' NOTE

The authors declare that there is no conflict of interest regarding the publication of this article. Authors confirmed that the paper was free of plagiarism.

6. REFERENCES

Abdul-Zahra, Z. J., and Rasheed, R. T. (2023). Preparation, characterization, and ninhydrin removal by Al_2O_3 and V_2O_5 nanoparticles. *Journal of Medicinal Chemistry and Sciences, 6*(2), 376–391.

Aldabagh, I. S., Saad, D. N., and Ahmed, E. I. (2024). Removal of methylene blue from aqueous solution by green synthesized silicon dioxide nanoparticles using sunflower husk. *Chemical Engineering Journal Advances, 18*, 100608.

Chaukura, N., Murimba, E. C., and Gwenzi, W. (2017). Synthesis, characterisation and methyl orange adsorption capacity of ferric oxide–biochar nanocomposites derived from pulp and paper sludge. *Applied Water Science, 7*(5), 2175–2186.

Chu, Q., Hoong, K., Hashim, M. A., Bashiri, H., Debord, J., Harel, M., and Bollinger, J.-C. (2023). The Flory–Huggins isotherm and water contaminant adsorption: Debunking some modeling fallacies. *Industrial and Engineering Chemistry Research, 62*(2), 1121–1131.

Deletic, A., and Wang, H. (2019). Water pollution control for sustainable development. *Engineering, 5*(5), 839–840.

Do, P. M. T., Phan, T. T. T., Nguyen, C. H., Downes, N. K., and Nguyen, L. X. (2023). Removal of anions PO_4^{3-} and methyl orange using Fe-modified biochar derived from rice straw. *Iranian Journal of Chemistry and Chemical Engineering, 42*(3), 821-834.

Ezzatfar, R., Dehghan, G., Amini, M., and Khataee, A. (2022). Synthesis of peroxidase-like V_2O_5 nanoparticles for dye removal from aqueous solutions. *Topics in Catalysis, 65*(5), 694–702.

Fathi, A., Asgari, E., Danafar, H., Salehabadi, H., and Fazli, M. M. (2024). A comprehensive study on methylene blue removal via polymer and protein nanoparticle adsorbents. *Scientific Reports, 14*(1), 29434.

Gong, R., Ye, J., Dai, W., Yan, X., Hu, J., Hu, X., Li, S., and Huang, H. (2013). Adsorptive removal of methyl orange and methylene blue from aqueous solution with finger-citron-residue-based activated carbon. *Industrial and Engineering Chemistry Research*, *52*(39), 14297-14303.

Hien, V. X., Dong, V. T., Vuong, D. D., and Chien, N. D. (2021). From microurchins to V_2O_5 nanowalls: Improved synthesis through vanadium powder and fast, selective adsorption of methylene blue. *Langmuir, 38*(1), 264–274.

Homaeigohar, S. (2020). The nanosized dye adsorbents for water treatment. *Nanomaterials, 10*(2), 1–42.

Iqbal, M. Z., Pal, P., Shoaib, M., and Abdala, A. A. (2017). Efficient removal of different basic dyes using graphene. *Desalination and Water Treatment, 68*, 226–235.

Jaseela, P. K., Garvasis, J., and Joseph, A. (2019). Selective adsorption of methylene blue (MB) dye from aqueous mixture of MB and methyl orange (MO) using mesoporous titania (TiO_2)–poly(vinyl alcohol) nanocomposite. *Journal of Molecular Liquids, 286*, 110908.

Jehad, A. M., Rasheed, R. T., Mansoor, H. S., Mohammed, M. N., Abdullah, T. A., Mansoor, A. S., Abdul-Zahra, Z. J., Hussein, M. A., Kułacz, K., and Abdullah, O. I. (2024). Preparation and characterization of vanadium pentoxide and nickel oxide nanoparticles and their use in removing tetracycline from water. *Topics in Catalysis, 68*(11), 1–15.

Juzsakova, T., Salman, A. D., Abdullah, T. A., Rasheed, R. T., Zsirka, B., Al-Shaikhly, R. R., Sluser, B., and Cretescu, I. (2023). Removal of methylene blue from aqueous solution by mixture of reused silica gel desiccant and natural sand or eggshell waste. *Materials*, *16*(4), 1618.

Khan, I., Saeed, K., Zekker, I., Zhang, B., Hendi, A. H., Ahmad, A., Ahmad, S., Zada, N., Ahmad, H., Shah, L. A., Shah, T., and Khan, I. (2022). Review on methylene blue: its properties, uses, toxicity and photodegradation. *Water*, *14*(2), 242.

Kolya, H., and Kang, C.-W. (2024). Toxicity of metal oxides, dyes, and dissolved organic matter in water: Implications for the environment and human health. *Toxics, 12*(2), 111.

Lv, S. W., Liu, J. M., Ma, H., Wang, Z. H., Li, C. Y., Zhao, N., and Wang, S. (2019). Simultaneous adsorption of methyl orange and methylene blue from aqueous solution using amino functionalized Zr-based MOFs. *Microporous and Mesoporous Materials*, *282*, 179-187.

Mahdy, S. A., and Al-Naseri, H. (2024). Effect of magnesium oxide nanoparticles (MgO) on wastewater treatment and electric current generation using microbial fuel cell technology. *Tikrit Journal of Engineering Sciences, 31*(2), 219–228.

Maryanti, R., Rahayu, N. I., Muktiarni, M., Al Husaeni, D. F., Hufad, A., Sunardi, S., and Nandiyanto, A. B. D. (2022). Sustainable development goals (SDGs) in science education: Definition, literature review, and bibliometric analysis. *Journal of Engineering Science and Technology, 17*(6), 161-181.

Mashhour, D. M., Ibrahim, S. M., Al-Hossainy, A. F., and Abd El-Aal, M. (2024). Glycogen-assisted biosynthesis of MnO_2 for adsorptive elimination of methylene blue from water. *Journal of Molecular Structure, 1313*, 138665.

Mubarokah, S. L., Anwar, S., Nisa, K., Miftah, H., Hastuti, A., and Nandiyanto, A. B. D. (2024). Bibliometrics study on agro-economy of biochar. *Journal of Engineering Science and Technology, 19*, 142-152.

Nandiyanto, A. B. D., Kurniawan, T., Bilad, M. R., and Farobie, O. (2025). Harnessing biomass for Sustainable Development Goals (SDGs): Definition, bibliometric, application, opportunities, and challenges. *Journal of Engineering Science and Technology, 20(4), 1047-1068.*

Nguyen, C. H., Fu, C.-C., and Juang, R.-S. (2018). Degradation of methylene blue and methyl orange by palladium-doped TiO_2 photocatalysis for water reuse: Efficiency and degradation pathways. *Journal of Cleaner Production, 202*, 413–427.

Nuraeni, A., Taba, P., Zakir, M., and Lakolo, L. (2023). Synthesis and characterization of mesoporous silica MCM-48 as dye adsorbent of methyl orange. *AIP Conference Proceedings, 2580*(1), 050028.

Obayomi, K. S., Lau, S. Y., Zahir, A., Meunier, L., Zhang, J., Dada, A. O., and Rahman, M. M. (2023). Removing methylene blue from water: A study of sorption effectiveness onto nanoparticles-doped activated carbon. *Chemosphere, 313*, 137533.

Ramutshatsha-Makhwedzha, D., Mavhungu, A., Moropeng, M. L., and Mbaya, R. (2022). Activated carbon derived from waste orange and lemon peels for the adsorption of methyl orange and methylene blue dyes from wastewater. *Heliyon, 8*(8), e09930.

Rasheed, R. T., Mansoor, H. S., Abdullah, T. A., Juzsakova, T., Al-Jammal, N., Salman, A. D., Al-Shaikhly, R. R., Le, P. C., Domokos, E., and Abdulla, T. A. (2021). Synthesis, characterization of V_2O_5 nanoparticles and determination of catalase mimetic activity by new colorimetric method. *Journal of Thermal Analysis and Calorimetry, 145*, 297–307.

Shankar, S., Kumar, Y., Sharma, N., Chandra, R., and Kumar, S. (2024). Disposable zirconium trisulfide–reduced graphene oxide modified conducting thread-based electrochemical biosensor for lung cancer diagnosis. *Bioelectrochemistry, 160*, 108801.

Sharma, P., Hussain, N., Borah, D. J., and Das, M. R. (2013). Kinetics and adsorption behavior of the methyl blue at the graphene oxide/reduced graphene oxide nanosheet–water interface: A comparative study. *Journal of Chemical and Engineering Data, 58*(12), 3477–3488.

Shi, Y., Song, G., Li, A., Wang, J., Wang, H., Sun, Y., and Ding, G. (2022). Graphene oxide-chitosan composite aerogel for adsorption of methyl orange and methylene blue: Effect of pH in single and binary systems. *Colloids and Surfaces A: Physicochemical and Engineering Aspects*, *641*, 128595.

Solehuddin, M., Nandiyanto, A. B. D., Muktiarni, M., Rahayu, N. I., Al Husaeni, D. N., Ragadhita, R., and Fiandini, M. (2025). Engineering research and scientific contributions at Universitas Pendidikan Indonesia: Trends, challenges, and future directions. *Journal of Engineering Science and Technology, 20*(3), 816-836.

Taquieteu, I. K., Dzoujo, H. T., Shikuku, V. O., Banenzoué, C., and Joh Dina, D. D. (2023). Fixed-bed adsorption of an azo dye (methyl orange) onto chemically and thermally regenerated activated carbons. *Journal of Chemistry, 2023*(1), 6677710.

Xie, S., Yang, Y., Gai, W. Z., and Deng, Z. Y. (2021). Oxide modified aluminum for removal of methyl orange and methyl blue in aqueous solution. *RSC Advances, 11*(2), 867–875.